

Astronomically tuned Plio–Pleistocene benthic $\delta^{18}\text{O}$ record from South China Sea and Atlantic–Pacific comparison

Jun Tian^{a,*}, Pinxian Wang^a, Xinrong Cheng^a, Qianyu Li^b

^a *Laboratory of Marine Geology, Tongji University, Shanghai 200092, PR China*

^b *Department of Geology and Geophysics, University of Adelaide, Adelaide, SA 5005, Australia*

Received 22 January 2002; received in revised form 23 July 2002; accepted 16 August 2002

Abstract

Based on benthic foraminiferal $\delta^{18}\text{O}$ from ODP Site 1143, a 5-Myr astronomical timescale for the West Pacific Plio–Pleistocene was established using an automatic orbital tuning method. The tuned Brunhes/Matuyama paleomagnetic polarity reversal age agrees well with the previously published age of 0.78 Ma. The tuned ages for several planktonic foraminifer bio-events also agree well with published dates, and new ages for some other bio-events in the South China Sea were also estimated. The benthic $\delta^{18}\text{O}$ from Site 1143 is highly coherent with the Earth's orbit (ETP) both at the obliquity and precession bands for the last 5 Myr, and at the eccentricity band for the last 2 Myr. In general, the 41-kyr cycle was dominant through the Plio–Pleistocene although the 23-kyr cycle was also very strong. The 100-kyr cycle became dominant only during the last 1 Myr. A comparison of the benthic $\delta^{18}\text{O}$ between the Atlantic (ODP 659) and the East and West Pacific (846 and 1143) reveals that the Atlantic–Pacific benthic oxygen isotope difference ratio ($\Delta\delta^{18}\text{O}_{\text{Atl-Pac}}$) displays an increasing trend in three time intervals: 3.6–2.7 Ma, 2.7–2.1 Ma and 1.5–0.25 Ma. Each of the intervals begins with a rapid negative shift in $\Delta\delta^{18}\text{O}_{\text{Atl-Pac}}$, followed by a long period with an increasing trend, corresponding to the growth of the Northern Hemisphere ice sheet. This means that all three intervals of ice sheet growth in the Northern Hemisphere were accompanied at the beginning by a rapid relative warming of deep water in the Atlantic as compared to that of the Pacific, followed by its gradual relative cooling. This general trend, superimposed on the frequent fluctuations with glacial cycles, should yield insights into the processes leading to the boreal glaciation. Cross-spectral analyses of the $\Delta\delta^{18}\text{O}_{\text{Atl-Pac}}$ with the Earth's orbit suggests that after the initiation of Northern Hemisphere glaciation at about 2.5 Ma, obliquity rather than precession had become the dominant force controlling the vertical structure or thermohaline circulation in the paleo-ocean.

© 2002 Elsevier Science B.V. All rights reserved.

Keywords: stable isotopes; astronomical time scale; South China Sea; Pliocene; Pleistocene; Atlantic Ocean; Pacific Ocean

1. Introduction

The last 5 Myr of paleoceanographic history is crucial to our understanding of the Earth's climate system. The final closure of the Panama Isthmus and the Indonesian seaway, further uplift of the Tibetan Plateau and the onset of major ice

* Corresponding author. Tel.: +86-21-65984878 or +86-21-65983207; Fax: +86-21-65988808.
E-mail address: ian.tianjun@263.net (J. Tian).

sheets in the Northern Hemisphere, a series of major events leading to the modern patterns of the Earth system, are located within this period of time. Deep sea sediments are the main carrier of high-resolution long-term records of Plio–Pleistocene ocean history, yet adequate isotopic sequences are rare in the literature. Up to now, only a few ODP sites provided continuous isotopic records of benthic foraminifera over the last 5 Myr with time resolution at the millennial scale. Of those, two are from the Eastern Pacific (ODP Sites 846 [1,2] and 849 [3]) and one from the Atlantic (ODP Site 659 [4]) (Table 1). Because of the great water depths and poor carbonate preservation, no long sequence is available from the Western Pacific, despite its undoubted significance.

The hemipelagic sediments from the South China Sea (SCS) are distinguished by high sedimentation rate and carbonate preservation. With the modern carbonate compensation depth at about 3500 m, the SCS offers a unique opportunity to collect from the region a high-resolution oxygen isotope record covering a long period of time. ODP Site 1143 from the SCS provides for the first time a high-resolution long-term isotopic record in the Western Pacific. As seen from Table 1, this is the only site in any ocean which has yielded complete records of benthic and planktonic isotope data covering the entire last 5 Myr.

2. Oceanographic settings of the SCS

The SCS, measuring 3.50×10^6 km² in area and 4.24×10^6 km³ in volume, is the largest marginal

sea of the Western Pacific. This is a semi-enclosed basin open to the Pacific only through the Bashi Strait with a sill depth of 2.6 km [5]. The Pacific Deep Water (1–4 km deep, temperature minimum in its bottom layer) and Pacific Intermediate Water (above the salinity minimum at 1 km depth) enter the SCS through the Strait and fill the 5377-m-deep basin, giving rise to a fairly uniform deep water structure there. The SCS Bottom Water under the sill depth (2600 m) has a stable temperature lower than 2.4°C, salinity of 34.6–34.7‰, and oxygen concentration around 2.5 ml/l, whereas the SCS Deep Water from 1 km to 2.6 km is fairly close to the Pacific Bottom Water in properties [6]. Cruise SONNE-95 to the SCS in 1994 measured CTD profiles at five stations, where all the curves show a uniform salinity, oxygen and temperature below 2.0–2.5 km depth. The 5-cm surface sediment temperatures in all 48 box cores also show a stable value of 2.4°C below 2 km depth [7].

Enclosed-type seas are advantageous for paleoceanographic studies because of their high sedimentation rates and tendency to amplify environmental changes. On the other hand, carbonate preservation in many of them is poor due to shallow sill depths, such as in the Sea of Japan (130 m) and the Mediterranean Sea (280 m). Thanks to the greater sill depth, the deeper waters in the SCS are well ventilated and connected with the open Pacific even during glacial times [8]. The resident time of the SCS Bottom Water is estimated to be as short as 76 years [6], and as a result, the oxygen component of the SCS below its sill depth is closely comparable to that of the Pacific Deep Water (from 1 km to 4 km deep). The deep water

Table 1

Long marine oxygen isotope sequences (only complete sequences with time spans longer than 5 Myr, resolution better than 5 kyr are shown)

Ocean	Site	Location	Water depth (m)	Age (Myr)	Sedimentation rate (cm/kyr)	Resolution (kyr)	F	Reference
West Pacific	1143	9°22'N, 113°17'E	2772	5	3.9	2.6 (P) 2.8 (B)	PB	This paper
East Pacific	846	3°06'S, 90°49'W	3296	6	4.2	2.5	B	[2]
	849	0°11'N, 110°31'W	3851	5	2.8	~4	B	[1]
Atlantic	659	18°05'N, 21°02'W	3070	5	2.9	~4	B	[4]

F: foraminifera; P: planktonic; B: benthic.

$\delta^{18}\text{O}$ record of the SCS is therefore representative of the Western Pacific.

3. Materials and methods

ODP Site 1143 from the southern SCS is located at $9^{\circ}21.72'\text{N}$, $113^{\circ}17.11'\text{E}$, at a water depth of 2772 m (Fig. 1). The site lies within the north-western part of the Dangerous Grounds or Nansha Islands area, a region of poorly charted islands and reefs on the southern continental slope of the SCS. To its south are the terrigenous deposits of the paleo-Sunda and Mekong rivers, with accumulation rates as high as 100–300 m/Myr, and to its north is the carbonate-rich region of the northernmost southern SCS margin with low sedimentation rates of only 10–20 m/Myr. Average linear sedimentation rates of 30–70 m/Myr and mass accumulation rates of 3–10 $\text{g}/\text{cm}^2/\text{kyr}$ are expected in areas close to this site [9,10].

The Pleistocene to upper Pliocene sediments recovered at Site 1143 consist mostly of olive, greenish, and light gray green and greenish gray clayey nannofossil mixed sediment, clay with nannofossils, and clay. Samples were from Holes 1143A, 1143B and 1143C at 10 cm apart, representing a time resolution of approximately 2 kyr for untuned records. They were combined to represent a complete section on a continuous compo-

site depth scale (mcd) by splicing high resolution (2 cm spacing) magnetic susceptibility and other physical properties records between 0 and 190.77 mcd from the advanced piston coring interval [11]. A total of 1992 samples of benthic foraminifers were measured for isotopes.

The preparation of samples and stable isotope analyses were performed in the Marine Geology Laboratory of Tongji University, Shanghai. Mud samples were soaked in tap water for 1–2 days after drying at 60°C in an oven, washed through a $63\text{-}\mu\text{m}$ sieve, dried at 60°C in the oven, then sieved to select foraminifers coarser than $150\text{ }\mu\text{m}$ for stable isotope analysis. Well preserved specimens (clean, intact, with no signs of dissolution) of the benthic foraminifers *Cibicides wuellerstorfi* or *Uvigerina peregrina* (when the former was not available) were chosen and washed in ethanol ($\geq 99.7\%$) in an ultrasonic bath at a frequency of 40 kHz three times, each time lasting 5–10 s. They were dried at 60°C in an oven for 5 h, moved to the sample vial in a Finnigan automatic carbonate device (Kiel III), reacted with *ortho*-phosphoric acid at 70°C to generate CO_2 , then transferred to and measured in a Finnigan MAT252 mass spectrometer. Precision was regularly checked with a Chinese national carbonate standard (GBW04405) and international standard NBS19; the standard deviation was 0.07‰ for $\delta^{18}\text{O}$ and 0.04‰ for $\delta^{13}\text{C}$. Measurements were made in the course of the year 2000. Conversion

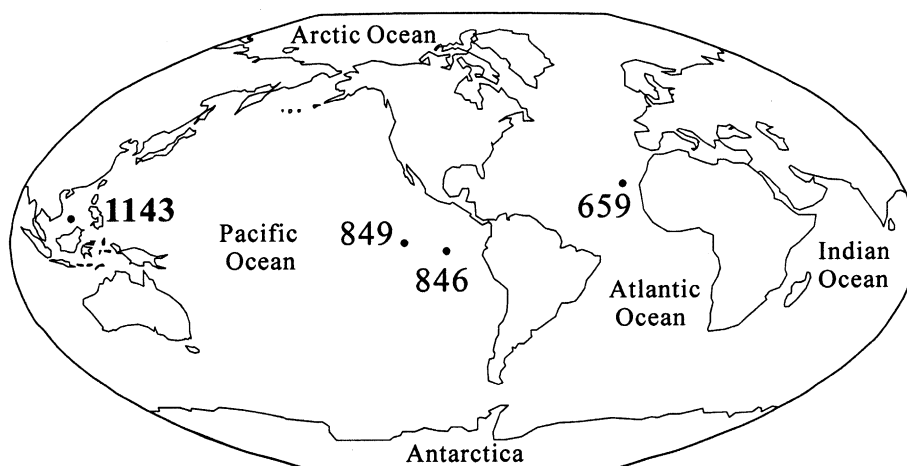


Fig. 1. Location map of ODP Site 1143, southern part of the SCS, and other ODP Sites with long isotope records.

to the international Pee Dee Belemnite (PDB) scale was performed using NBS19 and NBS18 standards. Following the standard of Shackleton and Hall [12], 0.64‰ was subtracted from the $\delta^{18}\text{O}$ values of *U. peregrina* and 0.9‰ was added to the $\delta^{13}\text{C}$ values, to make them comparable to the values of *C. wuellerstorfi*.

4. Stratigraphy of ODP Site 1143

4.1. Magnetostratigraphy and biostratigraphy

Because of the strong overprinting of paleomagnetic signals from all three holes at Site 1143, only the Brunhes/Matuyama paleomagnetic polarity reversal was identified in Sections 1143A–6H, at ~ 42.5 – 43.8 mcd and in 1143C–5H, at 43.2 mcd. In the initial report of ODP Leg 184 [11], the depth of 43.2 mcd was given as representing this polarity boundary. Generally the boundary is found in marine isotope stage (MIS) 19, with a commonly accepted age of 780 ka [13,14]. As the range of MIS 19 is between 42.04 and 43.00 mcd on our composite $\delta^{18}\text{O}$ curve (Fig. 2), this polarity

boundary correlates well with the isotopic records.

Post-cruise studies identified 14 planktonic foraminifer datum events for biostratigraphic resolution of 2–10 kyr of the last 5 Myr at ODP Site 1143. Table 2 shows the details of these bioevents, and their estimated ages from previous studies given mostly in Berggren et al. [15].

4.2. Oxygen isotope stratigraphy

The benthic $\delta^{18}\text{O}$ of ODP Site 1143 was plotted against depth down to 190.77 mcd, as shown in Fig. 2. The identification of MISs in 1143 was mainly based on the visual comparison of the benthic $\delta^{18}\text{O}$ curve of 1143 with that of a newly compiled 6-Myr $\delta^{18}\text{O}$ curve by Shackleton. This curve used the benthic oxygen isotope data of Core V19-30 [16] for 0–0.34 Ma, of ODP Site 677 [17] for 0.34–1.818 Ma, and of ODP Site 846 [2] for 1.811–6.0 Ma. Because of a similar ~ 3 -kyr resolution, the two curves can be directly compared. In this paper, we adopt the nomenclature of MISs used by Shackleton et al. [2] and Tiedemann et al. [4] and apply it to Site 1143.

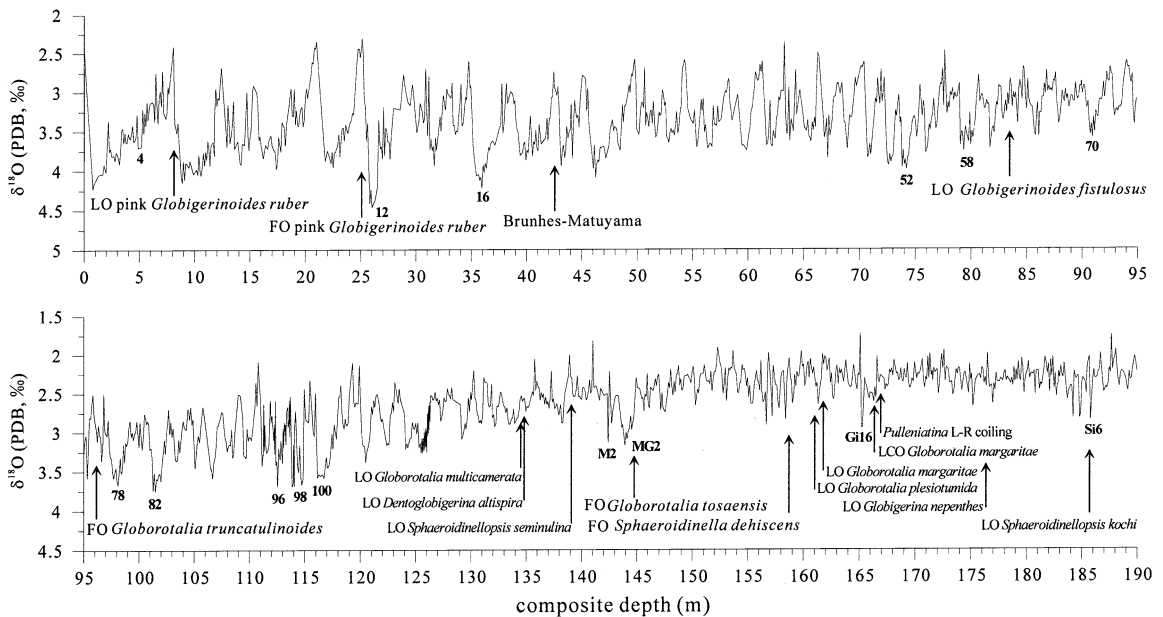


Fig. 2. Benthic foraminifer $\delta^{18}\text{O}$ record from ODP Site 1143 plotted against mcd. Isotopic values are from the benthic foraminifers *C. wuellerstorfi* and *U. peregrina*. The values of *U. peregrina* were adjusted by subtracting 0.64‰. Arrows denote paleomagnetic and biostratigraphic events. Some selected MISs are labeled.

Table 2
Ages of planktonic foraminiferal events estimated in this study of ODP Site 1143 and from previous studies

Event	Mean level (mcd)	Sample (mcd)	Age estimated (Ma)	Confidence	Previous age (Ma)
LO pink <i>Globigerinoides ruber</i>	8.07	8.07	0.124	high	0.12 [33]
FO pink <i>Globigerinoides ruber</i>	25.03	25.03	0.407	high	0.40 [15]
LO <i>Globigerinoides fistulosus</i>	83.40	83.40	1.729	high	1.77 [15]
FO <i>Globorotalia truncatulinoides</i>	96.09	96.09	2.031	high	2.00 [15]
LO <i>Globorotalia multicamerata</i>	134.71	134.76–0.05	3.038	moderate	3.09 [15]
LO <i>Dentoglobigerina altispira</i>	134.81	134.86–0.05	3.041	high	3.09 [15]
LO <i>Sphaeroidinellopsis seminulina</i>	138.01	138.06–0.05	3.138	high	3.12 [15]
FO <i>Sphaeroidinella dehiscens</i>	158.35	158.36+0.05	3.800	high	3.25–5.54 [34]
FO <i>Globorotalia tosaensis</i>	144.39	144.34+0.05	3.348	high	3.35 [15]
LO <i>Globorotalia plesiotumida</i>	161.05	161.10–0.05	3.823	moderate	3.77 [15]
LO <i>Globorotalia margaritae</i>	161.58	161.58	3.833	low	3.58 [15]
<i>Pulleniatina</i> left to right coiling	166.55	166.50+0.05	4.051	high	3.95 [15]
LCO <i>Globorotalia margaritae</i>	166.45	166.50–0.05	4.047	high	3.96 [15]
LO <i>Globigerina nepenthes</i>	176.32	180.75–4.43	4.586	low	4.20 [15]

FO, first occurrence; LO, last occurrence; LCO, last common occurrence. Mean datum level at mcd was adjusted between the sample in which a datum was located and the next sample in which it was not. Lower confidence on the estimated age was mainly because of rare specimens and a coarser sampling resolution.

An isotopically increasing trend from MIS MG2 to MIS 96, indicative of Northern Hemisphere ice sheet growth, is clearly distinguishable in our $\delta^{18}\text{O}$ curve. Isotopic events such as MIS Gi16 and MIS Si6 before the initiation of Northern Hemisphere glaciation, and MIS 96, 98, 100 and MG2 during Northern Hemisphere ice growth, are all easy to recognize. A total of 191 MISs from 1 down to T1 were identified between 0 and 190.77 mcd at Site 1143 (Fig. 2), which is assigned an age range of 0–5.02 Ma, slightly older than in the age model from the Initial Report [11].

5. Astronomical calibration of the timescale

5.1. Astronomical tuning

The initial age model of Site 1143 based on magnetostratigraphy and biostratigraphy is inadequate for high-resolution studies, particularly for climate responses to orbital forcing. Although a visual correlation of the 1143 isotopic curve to Shackleton's 6-Myr oxygen isotopic curve produced a satisfactory age model, tuning the benthic isotopic record directly to the Earth's orbit is a more direct procedure for the development of an

astronomical timescale, and may potentially yield greater chronological precision.

Since the pioneering work of Milankovitch [18] and Hays et al. [19], revealing the close cause and effect relationship between the Earth's orbital geometry and climatic variance, orbitally tuned timescales have been established by tuning climatic variances such as $\delta^{18}\text{O}$ [20], eolian dust [4], grain size [21] and γ -ray attenuation porosity evaluator [22] to Earth's orbital elements including eccentricity, obliquity and precession. The astronomical solution of these elements has been developed mainly by Berger and Loutre [23] and Laskar [24], using methods differing only in minor details over the last 5 Myr. Here, the astronomical solution of Laskar [24] for the obliquity and precession were used as the tuning target.

The phase relationship between orbital forcing and foraminiferal $\delta^{18}\text{O}$ for the Pleistocene has been well established, with $\delta^{18}\text{O}$ minima tending to lag the Northern Hemisphere 65° summer insolation maxima by $\sim 69^\circ$ at the obliquity band and $\sim 78^\circ$ at the precession band, equivalent to 7.8 kyr and 5 kyr respectively [25]. Because $\delta^{18}\text{O}$ is globally correlative at least for the Pleistocene, tuning $\delta^{18}\text{O}$ to obliquity or precession may accurately reflect the phase lead and lag relationship

between climate variables from globally distributed sites. This phase relationship, however, is not yet well established for the pre-Pleistocene. Indeed, Clemens et al. [26] found a non-stationary precession phase for the Asian monsoons during the Pliocene–Pleistocene and Chen et al.'s [27] experiments indicate very small differences in the phase lags of various cycles with the changes in time constant from 17 to 8 kyr which are variable parameters for ice sheet response to external forcing. In this study, an 8-kyr lag for the obliquity curve and 5-kyr lag for the precession curve from Laskar [24] (1,0) were used.

Clemens [28] pointed out that the 41-kyr component of $\delta^{18}\text{O}$ is the most likely climate variable to be globally correlative and the most stable in phase relative to orbital forcing [28]. The final age model of Site 1143 as seen from Fig. 3 was obtained by repeatedly tuning the initial age model to obliquity until coherencies between the filtered $\delta^{18}\text{O}$ signals and orbital signals reached a maxi-

imum fit. An automatic orbital tuning method which utilizes the Dynamic Optimization technique was used during the process of tuning [29].

5.2. Cross-spectral analyses of $\delta^{18}\text{O}$ and ETP

A simple but very effective means of assessing the age model is to use cross-spectral analysis to analyze the spectra against a target curve. The sum of normalized eccentricity (e), normalized obliquity (t) and negative normalized precession (p) from the Laskar [24] (1,0) astronomical solution was used to set the target curve, as the ETP sum ($=e+t-p$) reflects the characteristics of these orbital elements of the Earth.

The cross-spectral analyses of benthic $\delta^{18}\text{O}$ with ETP were performed separately for five intervals: 0–1 Ma, 1–2 Ma, 2–3 Ma, 3–4 Ma and 4–5 Ma, and the results are shown in Fig. 4 and Table 3. The $\delta^{18}\text{O}$ spectra are highly coherent with ETP at the 41-kyr obliquity band and 23- and 19-kyr pre-

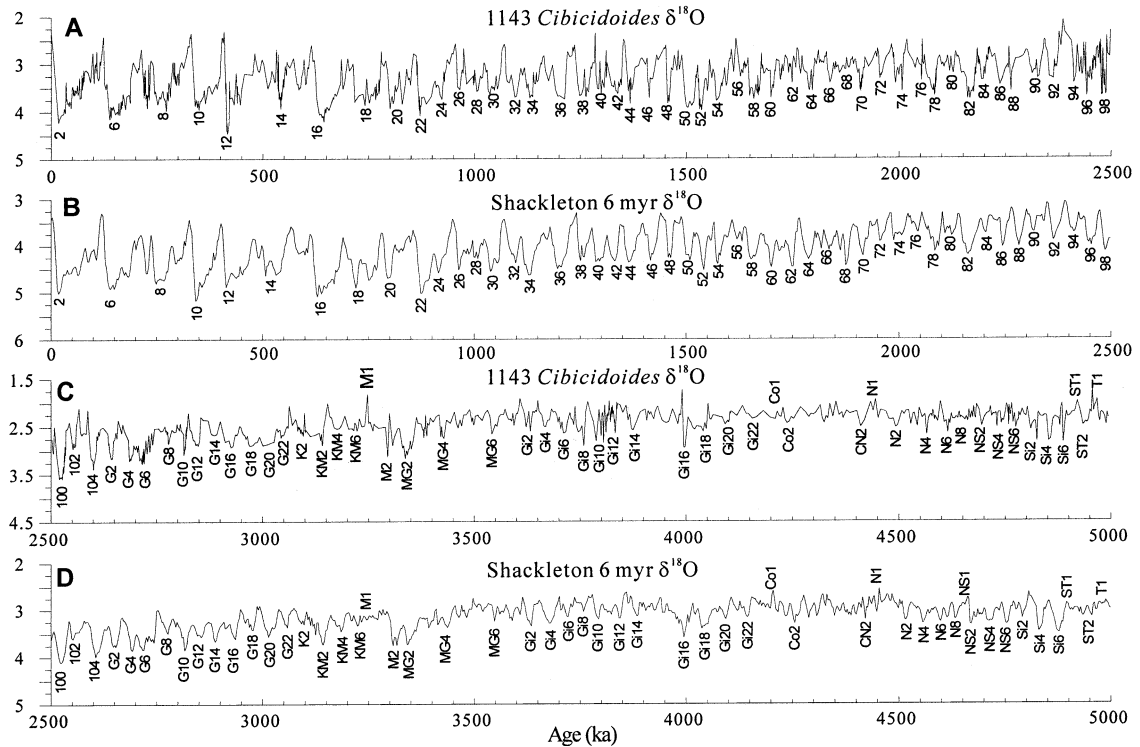


Fig. 3. Correlation of ODP 1143 $\delta^{18}\text{O}$ data with Shackleton's 6-Myr composite $\delta^{18}\text{O}$ curve [2,16,17]. Benthic foraminifer $\delta^{18}\text{O}$ curves from 0 to 2.5 Ma: (A) ODP 1143, (B) composite $\delta^{18}\text{O}$ curve; from 2.5 to 5.0 Ma: (C) ODP 1143, (D) composite $\delta^{18}\text{O}$ curve.

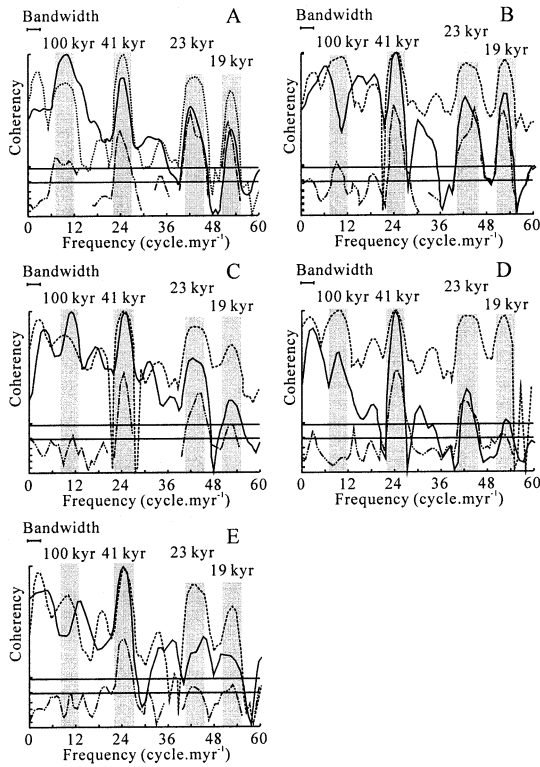


Fig. 4. Cross-spectral analyses of $\delta^{18}\text{O}$ with ETP for different time intervals: (A) 0–1 Ma; (B) 1–2 Ma; (C) 2–3 Ma; (D) 3–4 Ma; (E) 4–5 Ma. ETP is the combination of normalized eccentricity, obliquity and negative precession derived from the Laskar [24] (1,0) solution. Solid lines: $\delta^{18}\text{O}$; dashed lines: ETP; dot-dashed lines: coherency. Spectral densities are normalized and plotted on a log scale. The coherency spectra are plotted on a hyperbolic arctangent scale. Lower and upper horizontal lines show the non-zero coherency at the 80% and 95% levels respectively. Note the high coherency between $\delta^{18}\text{O}$ and ETP over 5 Myr at the obliquity (41 kyr) and two precessional bands (23 kyr and 19 kyr).

cession bands with >95% non-zero coherency. Only between 4 and 5 Ma does the coherency between these two time series drop to the 80–95% level. The spectral densities of 100-kyr, 23-kyr and 19-kyr periodicities in $\delta^{18}\text{O}$ increase significantly through time, as do their corresponding coherencies. The 41-kyr cycles of $\delta^{18}\text{O}$ remain strong throughout the whole section and the coherency at this band is high during each of the time intervals. This indicates that the 41-kyr component of $\delta^{18}\text{O}$ is the dominant cycle that can be correlated globally. At about 1 Ma, a distinct transition of the dominant cycles from 41 kyr to 100 kyr occurred, the so-called mid-Pleistocene revolution [30,31]. The 100-kyr component was unstable before 1 Ma, and became stabilized to pronounced only after the mid-Pleistocene event (Fig. 4). The 23-kyr and 19-kyr components are constantly strong and remain highly coherent with ETP in the whole $\delta^{18}\text{O}$ record. Similarly strong variations in $\delta^{18}\text{O}$ spectra on the precession band have also been found in the Atlantic [4], eastern equatorial Pacific [2,13], and Indian oceans [27,32]. This highlights the importance of any tropical precession cycles that might have introduced variance into the local climate system.

5.3. Comparison of filtered components of $\delta^{18}\text{O}$ with obliquity and precession

Another convenient means of assessing the age model is to compare the filtered 41-kyr component of $\delta^{18}\text{O}$ with the lagged obliquity and compare the filtered 23-kyr component of $\delta^{18}\text{O}$ with the lagged precession, as shown in Fig. 5. Gener-

Table 3
Cross-spectral phase relationship and coherency between Site 1143 $\delta^{18}\text{O}$ and ETP

Time interval	100 kyr (eccentricity)		41 kyr (obliquity)		23 kyr (precession)		19 kyr (precession)	
	coherency	phase	coherency	phase	coherency	phase	coherency	phase
0–1 Ma	0.879	-9.4 ± 15.1	0.9765	-66 ± 6.3	0.9737	-80.5 ± 6.6	0.9822	-86.8 ± 5.4
1–2 Ma	0.7789	-21.9 ± 21.8	0.9924	-55.4 ± 3.5	0.9654	-73.9 ± 7.6	0.9888	-94 ± 4.3
2–3 Ma	0.6193	-40.6 ± 32.2	0.9854	-58.1 ± 4.9	0.953	-78 ± 9	0.8509	-102.5 ± 17
3–4 Ma	0.3641	60.6 ± 51.8	0.9858	-69.9 ± 4.8	0.9402	-75.8 ± 10.2	0.7385	-95.6 ± 24.4
4–5 Ma	0.6634	145 ± 29.3	0.9772	-67 ± 6.2	0.7641	-60.1 ± 22.8	0.7681	-26.5 ± 22.5

Test statistics for non-zero coherency at 80% level = 0.707267.

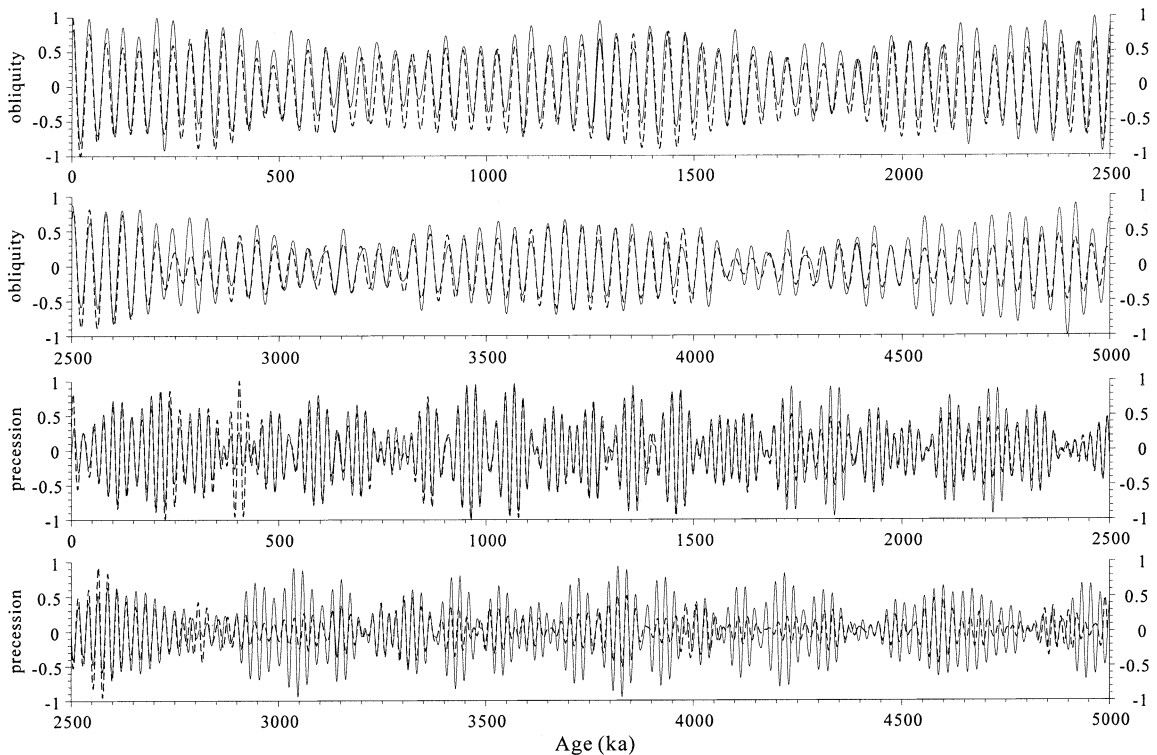


Fig. 5. Site 1143 $\delta^{18}\text{O}$ record filtered at the obliquity (41-kyr) and precession (23-kyr) bands (solid lines) compared with orbital obliquity (8-kyr lagged) and precession (5-kyr lagged) (dashed lines). The Tukey method in [29] was used for filtering. Band-pass filters with central frequencies of 0.02439 and 0.04762 kyr^{-1} and bandwidths of 0.040 and 0.015 kyr^{-1} were used to pick up the 41-kyr and 23-kyr components of the oxygen isotope time series.

ally, good matches exist between the filtered signals and the obliquity and precession except for some minor discrepancies in several short time intervals. The 41-kyr component synchronously changes both in phase and in amplitude with the lagged obliquity. The filtered 23-kyr component from 0 to 2.8 Ma changes synchronously with the lagged precession both in phase and in amplitude, except during a short time interval around MIS 12, ~ 400 ka. At Site 1143, in the southern SCS, the MIS 12 interval was recorded as a severe glacial period by some heaviest benthic and planktonic foraminiferal $\delta^{18}\text{O}$ values, exceeding those at other sites within the SCS, such as ODP Site 1146, and outside the SCS. It is still not known what mechanism caused the discrepancy between the great amplitudes in the filtered 23-kyr component of benthic $\delta^{18}\text{O}$ around MIS 12 and the small fluctuations of precession. During

the time intervals 2.8–2.9 Ma, 3.95–4.3 Ma, and 4.65–5.0 Ma, the filtered 23-kyr components do not co-vary with the precession, sometimes even changing to an opposite direction. This may be attributed to the tuning strategy, because any good match between the filtered 41-kyr components of climate indices and the obliquity in the early Pliocene appears to be possible only at the expense of failed matches between the filtered 23-kyr components and the precession. It seems that only in the Pleistocene and late Pliocene can the filtered 41-kyr and 23-kyr signals of climate indices be matched with orbital elements both in the phase and in the amplitude.

5.4. Estimated ages of paleomagnetic reversal and planktonic foraminifer events

After tuning the Brunhes/Matuyama boundary

of Site 1143 at 42.5 mcd shows an age of 780 ka, coinciding completely with the widely accepted chronology, and helping to confirm the reliability of our astronomical timescale for Site 1143.

The estimated ages of the planktonic foraminiferal events identified in Site 1143 are shown in Table 2. Generally, there is good agreement between the ages obtained in this study and those published previously. For example, the last occurrence (LO) of pink *Globigerinoides ruber* was dated at 0.12 Ma by Thompson et al. [33], and in this study an age of 0.124 Ma was determined for this event. Judging from the high-resolution $\delta^{18}\text{O}$ record presented here, this new age is considered to be more accurate at least for the SCS region. However, there are discrepancies between ages estimated for other, especially older, bio-events. Differences of 2–50 kyr were likely caused by the limits of sampling resolution, although we are confident that our sampling resolution is mostly higher than in those studies quoted in Table 2. Discrepancies larger than 50 kyr probably reflect the influence of local physiochemical parameters, rarity of specimens due to dissolution or poor preservation, and/or different species con-

cepts employed in species identification. Moreover, stepwise occurrences and extinctions are not uncommon among planktonic foraminifers, especially if they are from different faunal zones. New ages for individual datum events emerge from more detailed work on more expanded complete sections and better preserved material. Therefore, it is not surprising that many estimated ages for microfossil events are subject to modifications and revisions in the light of new findings. The LO of *Globorotalia margaritae* has been dated at 3.4 Ma by Berggren et al. [34], at 3.58 Ma by Berggren et al. [15], and at ~ 4.3 Ma from the South Pacific [35]. At Site 1143, this species is rare above 166 mcd, and its LO, located at 161.58 mcd, would bear an age of ~ 3.833 Ma on the new astronomic timescale (Table 2). The age for LO *Globigerina nepenthes* has also been changed from 3.9 Ma [34] to 4.2 Ma [15]. It is here estimated to be at 4.586 Ma, although our confidence in this estimate is comparatively low because preservation was poor to moderate close to 176 mcd, where the datum was found, and because the sampling resolution at this level is low, > 5 kyr (Table 2).

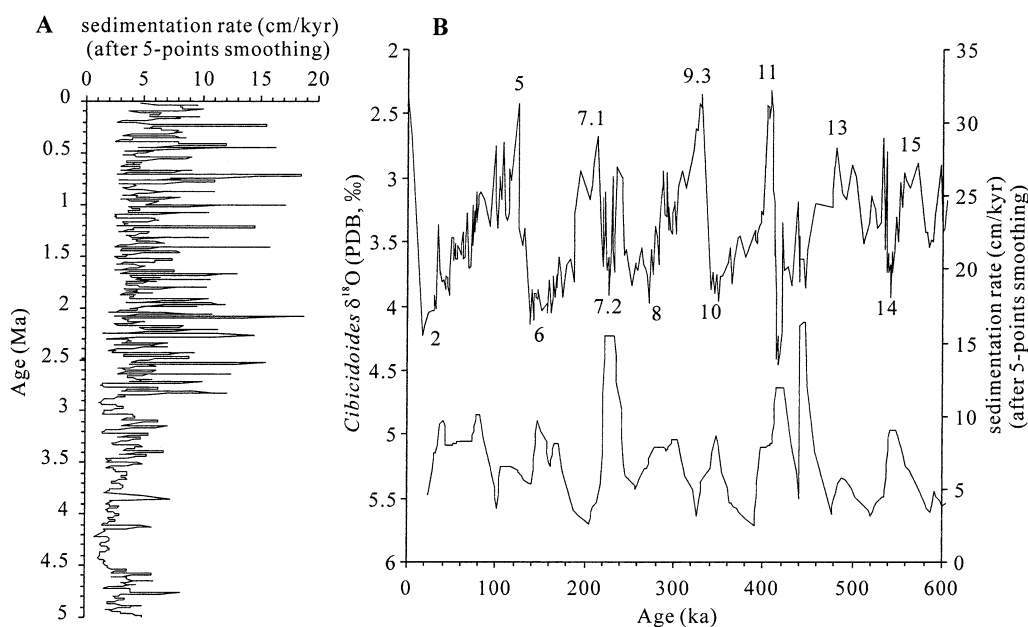


Fig. 6. Sedimentation rate of ODP Site 1143 after five-point running smoothing. (A) sedimentation rate in the last 5 Myr. (B) Sedimentation rate in the last 600 kyr. The numbers labeled in B indicate the MISs.

5.5. Accumulation rate

After five-point smoothing, the average linear sedimentation rate is ~ 57.2 m/Myr. Obviously from Fig. 6, 2.9 Ma is a threshold for the sedimentation rate in the location of Site 1143. Before this time, the average sedimentation rate is ~ 39.5 m/Myr, with a small amplitude of ~ 50 m/Myr. After this time, the average sedimentation rate jumped to ~ 65.4 m/Myr, with an amplitude as large as 200 m/Myr. The most interesting is that the sedimentation rate in glacial is nearly twice as high as in the adjacent interglacials (Fig. 6). As seen from Fig. 6A, the accumulation rate in interglacial times is around 40–50 m/Myr, whereas it reaches 100–200 m/Myr in glacial times, nearly two to four times as high as during interglacials, especially after 2.9 Ma. Such a relationship is clearly presented in Fig. 6B in the past 600 kyr.

6. Atlantic–Pacific comparison

6.1. Comparison

Since the recognition of the significance of thermohaline circulation in the climate system, the deep water comparison between the Atlantic and Pacific has become one of the foci of paleoceanography. Shackleton et al. [16] were the first to use the benthic foraminiferal isotopic curves from the East Pacific and North Atlantic to explore the deep water history of the global ocean. They found much larger-amplitude $\delta^{18}\text{O}$ fluctuations in the glacial cycles over the past 140 kyr in the Atlantic than in the Pacific. Later, the difference was ascribed to changes in temperature [36] and sources of deep water [37]. The modern deep water between 2 and 4 km in the North Atlantic is nearly 1.2°C warmer than in the Central Pacific, and the benthic $\delta^{18}\text{O}$ there is slightly lighter. During the last glacial maximum, however, the benthic $\delta^{18}\text{O}$ gradient between the two oceans was reversed, and the Pacific values were lighter by 0.1–0.2‰ than in the Atlantic [37], implying more significant deep water cooling (about 2.0°C) in the Atlantic than in the Pacific ($\sim 1.1^\circ\text{C}$ [36]). This contrast in the late Quaternary oceans is

generally attributed to the glacial reduction in production of North Atlantic Deep Water.

However, it remains unclear whether this feature also applies to earlier stages. Tiedemann et al. [4] and Mix et al. [3] compared benthic $\delta^{18}\text{O}$ records from the Atlantic and Pacific over the last 2.5–3.5 Ma and found exceptional coherency between the two, but did not focus on their differences. With the three long sequences of high-resolution (2.5–4.0-kyr) benthic $\delta^{18}\text{O}$ records available, the time is ripe for a comparison between the two oceans over the last 5 Myr. We calculated the difference between the benthic $\delta^{18}\text{O}$ records of ODP Site 659 from the North Atlantic and Sites 846 and 1143 from the East and West Pacific, hereinafter referred to as $\Delta\delta^{18}\text{O}_{659-846}$ and $\Delta\delta^{18}\text{O}_{659-1143}$.

To accomplish the correlation of Site 659 with Site 1143 and Site 846, the benthic $\delta^{18}\text{O}$ variations of 659 and 846 were visually correlated to those of Site 1143. To avoid high-frequency noise, the $\delta^{18}\text{O}$ records vs. age of Site 1143 were firstly smoothed, using a least square smoothing method with five points. The $\delta^{18}\text{O}$ records vs. depth of Sites 659 and 846 were also smoothed with the same method. The new age models for Sites 659 and 846 were then applied to the smoothed $\delta^{18}\text{O}$ records. To calculate the $\delta^{18}\text{O}$ difference, the $\delta^{18}\text{O}$ records of the three sites were linearly interpolated with a 4-kyr step.

As discussed above, the bottom water in the SCS below 2600 m is quite uniform in its properties. Our recent measurements show that benthic $\delta^{18}\text{O}$ below 2600 m in SCS varies only slightly from 2.40‰ to 2.65‰, a smaller difference than between similar depths in the open Pacific. Thus, the core top benthic $\delta^{18}\text{O}$ at 1143 (2.341‰) is lighter than that at 846 (2.74‰), although the difference can partly be ascribed to the greater water depth of the latter site (3296 m) as opposed to Site 1143 (2772 m). In sum, Site 1143 should represent the upper part, whereas Site 846 is representative of the lower part of the Pacific deep water (2–4 km). Therefore, the similar pattern of the two curves $\Delta\delta^{18}\text{O}_{659-846}$ and $\Delta\delta^{18}\text{O}_{659-1143}$ shown in Fig. 6 indicates general changes in the deep water $\delta^{18}\text{O}$ gradients between Atlantic and Pacific. Here we will focus on major trends of the

curves but not details, partly because slight differences are possible in mass spectrometer calibration between laboratories. Also, ODP core tops are often spoiled by the drilling process.

6.2. Results

A prominent feature in Fig. 6 are the mostly positive values of $\Delta\delta^{18}\text{O}_{659-1143}$ and $\Delta\delta^{18}\text{O}_{659-846}$ before 3.5 Ma. In other words, the Atlantic benthic $\delta^{18}\text{O}$ was heavier than that in the Pacific

between 3.5 and 5.0 Ma in our records. During this time interval, the $\delta^{18}\text{O}$ values of the Atlantic Site 659 are basically heavier than those of Site 1143 in the Pacific, except for some warm stages such as Gi17 with a $\delta^{18}\text{O}$ spike at Site 659 (Fig. 6). $\Delta\delta^{18}\text{O}_{659-1143}$ averages 0.111‰ during this period, whereas the difference between 659 and 846 ($\Delta\delta^{18}\text{O}_{659-846}$) then was less significant, with an average of 0.059‰. In general, the inter-oceanic oxygen isotopic fractionation during the early–middle Pliocene was opposite to the modern pat-

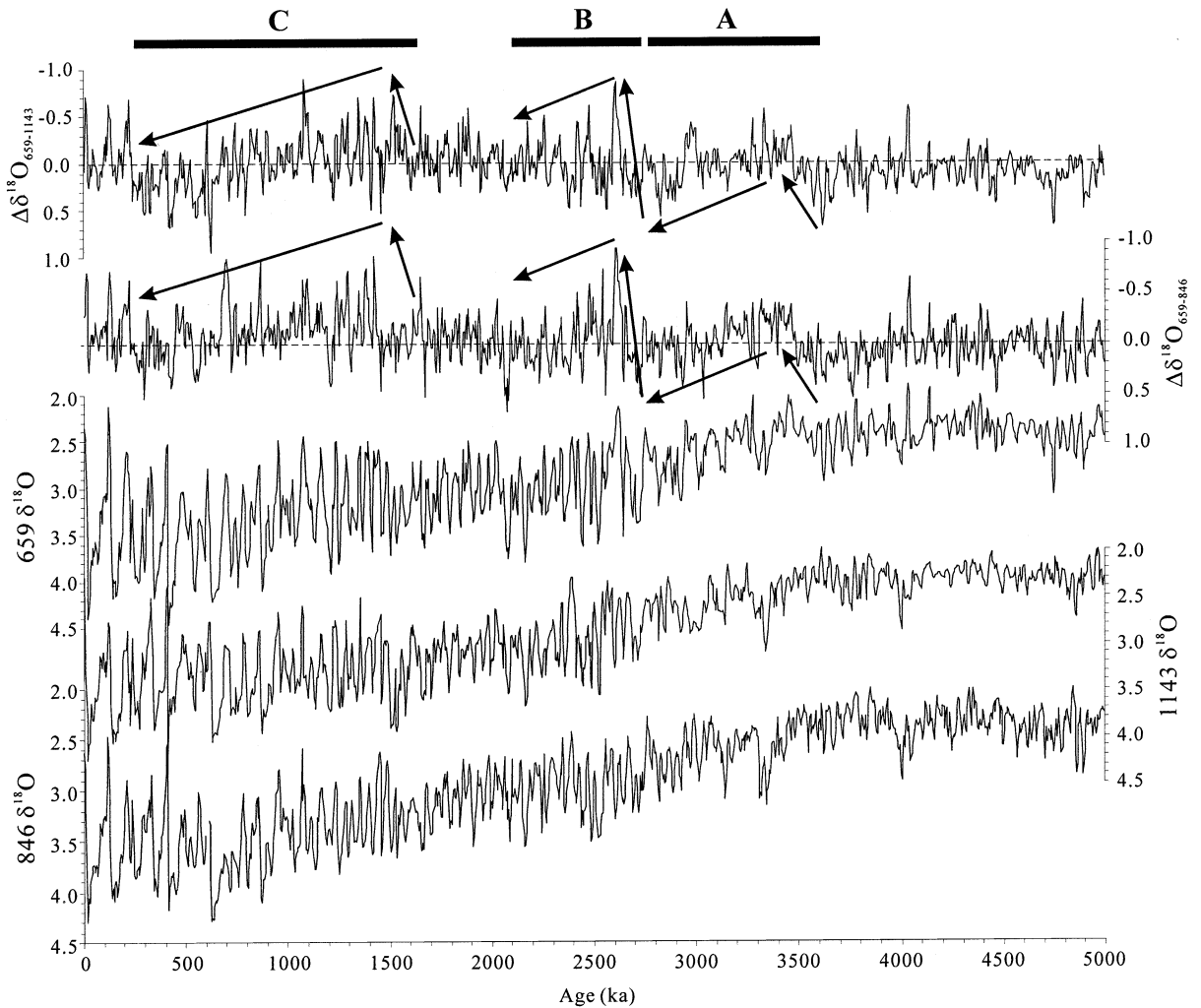


Fig. 7. Comparison of benthic $\delta^{18}\text{O}$ between the Atlantic and the East and West Pacific. The lower panels show benthic $\delta^{18}\text{O}$ records for the past 5 Myr of ODP Sites 846, 1143 and 659. The upper panels are benthic $\delta^{18}\text{O}$ difference between the Atlantic Site 659 and the Pacific Sites 846 and 1143. The black solid lines denote three time intervals: (A) 3.6–2.7 Ma, (B) 2.7–2.1 Ma, and (C) 1.5–0.25 Ma. Arrows indicate increasing or decreasing trends of the $\Delta\delta^{18}\text{O}_{\text{Atl-Pac}}$.

tern. With other conditions assumed to be equal, this would mean warmer deep water in the Pacific than in the Atlantic during the middle Pliocene. The deep water structure of the oceans was also more stable, judging from the smaller amplitude of fluctuation of benthic $\delta^{18}\text{O}$ than in the Pleistocene.

Fig. 7 shows three time intervals with an increasing trend in both $\Delta\delta^{18}\text{O}_{659-1143}$ and $\Delta\delta^{18}\text{O}_{659-846}$: (A) 3.6–2.7 Ma, (B) 2.7–2.1 Ma, and (C) 1.50–0.25 Ma. Each of the intervals begins with a rapid negative shift in Atlantic–Pacific difference of benthic $\Delta\delta^{18}\text{O}$ ($\Delta\delta^{18}\text{O}_{\text{Atl-Pac}}$), followed by a long period with an increasing trend of $\Delta\delta^{18}\text{O}_{\text{Atl-Pac}}$. A remarkable fact is that all the intervals correspond to growth phases of the Northern Hemisphere ice sheet, as seen from the $\delta^{18}\text{O}$ curves in Fig. 6. Thus, $\Delta\delta^{18}\text{O}_{\text{Atl-Pac}}$ experienced a decrease by $\sim 0.5\%$ within some 0.2 Myr, from 3.6 to 3.4 Ma, then gradually became heavier until the next negative shift at ~ 2.7 Ma. This interval A roughly corresponds to the onset of the Northern Hemisphere ice sheet formation [2]. Interval B began with a more drastic negative shift of $\Delta\delta^{18}\text{O}_{\text{Atl-Pac}}$ between 2.7 and 2.55 Ma, and its increase from 2.55 Ma to 2.1 Ma covers the onset of loess accumulation in China [38]. The beginning of the next interval, C, at 1.5 Ma coincided with the onset of the 100-kyr cyclicity in oxygen isotope records [39] implying the transition to a new phase in the Pleistocene glacial cycles. Then the trends increase until about 0.2 Ma when the fluctuations of inter-oceanic isotopic fractionation reached an unprecedented scale.

If the Atlantic–Pacific difference of benthic $\delta^{18}\text{O}$ denotes deep water temperature difference between the two oceans, then each of the major steps of the Northern Hemisphere ice sheet growth began with a rapid warming of the deep water in the Atlantic as compared with that in the Pacific, followed by a gradual decrease in contrast.

6.3. Interpretation

It is well accepted that differences in benthic carbon isotopes are indicative of deeper water masses and hence thermohaline circulation in

the ocean. Meanwhile, the differences in benthic oxygen isotopes are related not only to water masses, but are also sensitive to water temperature. Therefore, a comparison of benthic $\delta^{18}\text{O}$ between different sites may provide additional constraints for the reconstruction of vertical structures in the paleo-ocean [36,37]. An example is the finding of a thermocline near a depth of 2000 m during the Last Glacial Maximum on the Ontong–Java Plateau, Western Pacific, on the basis of $\Delta\delta^{18}\text{O}$ differences between sites [40].

The 5-Myr comparison of deep water $\delta^{18}\text{O}$ underscores the role of the boreal ice sheet in the global climate system. Before the onset of Northern Hemisphere glaciation at about 3.4 Ma, the deep water structure of the ocean was less variable, and the deep water in the Atlantic was apparently cooler than that in the Pacific. From 3.4 Ma onwards, the inter-oceanic isotopic fractionation became prominent, and all three intervals of ice sheet growth were accompanied at the beginning by a rapid relative warming of deep water in the Atlantic as compared to that in the Pacific, followed by its gradual cooling. This general trend, superimposed on the frequent fluctuations of glacial cycles, should throw some light on the initiation of Northern Hemisphere glaciation. Certainly, salinity might also contribute to the isotope gradient changes between oceans. However, with the poor knowledge about paleo-salinity no speculation on salinity is made in the present study.

To improve our understanding of the orbital control of the inter-oceanic fractionation, we conducted cross-spectral analyses of the Atlantic–Pacific $\delta^{18}\text{O}$ difference with ETP from two time intervals, 0–2.5 Ma and 2.5–5.0 Ma. It is obvious from Fig. 8 that prior to 2.5 Ma, marked concentrations of variance were present in precession and eccentricity bands, with high coherency against ETP in the precession band, but no concentration of variance in the obliquity band was recorded. In the interval 0–2.5 Ma, well-marked spectral peaks can be observed at eccentricity, obliquity and precession frequencies that are highly coherent with ETP, but the power of the spectrum and the coherency with ETP decreased in the precession band compared to the interval

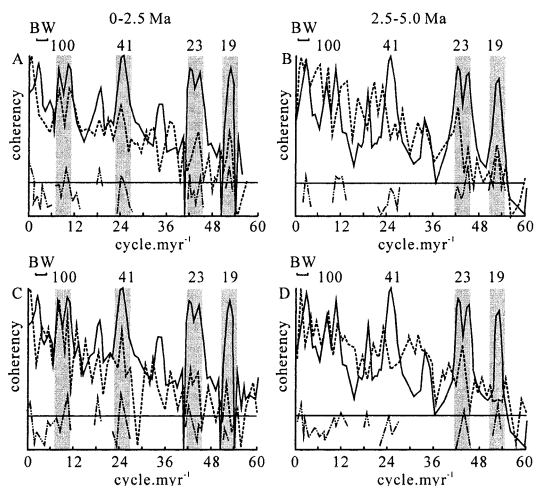


Fig. 8. Cross-spectral analyses between the Earth's orbits (ETP) and the benthic $\delta^{18}\text{O}$ difference of the Atlantic and the Pacific ($\Delta\delta^{18}\text{O}_{\text{Atl-Pac}}$). (A) ETP vs. $\Delta\delta^{18}\text{O}_{659-1143}$ (0–2.5 Ma); (B) ETP vs. $\Delta\delta^{18}\text{O}_{659-1143}$ (2.5–5.0 Ma); (C) ETP vs. $\Delta\delta^{18}\text{O}_{659-846}$ (0–2.5 Ma); (D) ETP vs. $\Delta\delta^{18}\text{O}_{659-846}$ (2.5–5.0 Ma). Solid lines: ETP; dotted lines: $\Delta\delta^{18}\text{O}_{659-1143}$ or $\Delta\delta^{18}\text{O}_{659-846}$; dash-dotted lines: coherency (on hyperbolic arc-tangent scale). Horizontal lines denotes non-zero coherency at the 80% level. Shaded areas highlight main Milankovitch cycles recorded in the spectrum.

2.5–5.0 Ma. These cross-spectrum results clearly indicate that after the initiation of Northern Hemisphere glaciation at about 2.5 Ma obliquity rather than precession became the dominant force controlling the vertical structure or thermohaline circulation in the paleo-ocean.

7. Conclusions

1. An astronomically calibrated timescale over the last 5 Myr is developed on the basis of ODP Site 1143, southern SCS, by tuning the benthic $\delta^{18}\text{O}$ to obliquity. This is the first high-resolution (2.8-kyr on average) long-term isotope stratigraphic sequence in the West Pacific region.
2. The cross-spectral relationship between ODP Site 1143 benthic $\delta^{18}\text{O}$ and the Earth's orbit clearly demonstrates a high coherency at obliquity (41-kyr) and precession (23-kyr and 19-kyr) bandwidths throughout the last 5 Myr. Only after 1 Ma was the benthic $\delta^{18}\text{O}$ coherent

with ETP at the eccentricity (100-kyr) bandwidth.

3. A comparison of the benthic $\delta^{18}\text{O}$ records between the Atlantic and the East and West Pacific reveals three time intervals with an increasing trend of inter-oceanic difference $\Delta\delta^{18}\text{O}_{\text{Atl-Pac}}$: 3.6–2.7 Ma, 2.7–2.1 Ma and 1.5–0.25 Ma, all corresponding to growth phases of the Northern Hemisphere ice sheet. Taking $\Delta\delta^{18}\text{O}_{\text{Atl-Pac}}$ as temperature difference, this would mean that the three intervals of boreal ice sheet growth were accompanied at the beginning by a rapid relative warming of deep water in the Atlantic as compared to that of the Pacific, followed by its gradual cooling. This general trend, superimposed on glacial cycles, should throw some light on the formation process of the Northern Hemisphere glaciation.
4. The cross-spectral analyses of the $\Delta\delta^{18}\text{O}_{\text{Atl-Pac}}$ with the Earth's orbits reveals that after the initiation of Northern Hemisphere glaciation at about 2.5 Ma obliquity rather than precession became the dominant force controlling the vertical structure of thermohaline circulation in the paleo-ocean.

8. Data

All data of the benthic $\delta^{18}\text{O}$ from ODP Site 1143 will be available from the first author (J.T.). The ASCII file contains composite depth, age and oxygen isotope data from *C. wuellerstorfi* or *U. peregrina*.

Acknowledgements

This research used samples provided by the Ocean Drilling Program (ODP). ODP is sponsored by the US National Science Foundation (NSF) and participating countries under management of Joint Oceanographic Institutions (JOI), Inc. Funding for this research was provided by the NNSFC (Grant 4999560) and NKBRSF (Grant G2000078500). Q.L. was supported by the Australian Research Council. We especially

thank Zhongli Ding and Zhiwei Yu for providing us with the tuning programs on which this study was based. Warren Prell is acknowledged for introducing the authors to statistical approaches to isotopic data during his visit and lectures in Shanghai. We also benefited greatly from discussions with Steve Clemens and from his comments on an early version of the manuscript. Cross-spectral analyses were performed using the ARAND program supplied generously by Philip Howell of Brown University. Li Baohua identified several planktonic foraminifer datums. A. Berger and S. Crowhurst reviewed the manuscript and offered valuable comments. [BOYLE]

References

- [1] A.C. Mix, J. Le, N.J. Shackleton, Benthic foraminiferal stable isotope stratigraphy of site 846: 0–1.8 Ma, in: N.G. Pisias, L.A. Mayer, T.R. Janecek, A. Palmer-Julson, T.H. van Andel (Eds.), Proc. ODP Sci. Results 138 (1995) 839–854.
- [2] N.J. Shackleton, N.J. Hall, D. Pate, Pliocene stable isotope stratigraphy of site 846, in: N.G. Pisias, L.A. Mayer, T.R. Janecek, A. Palmer-Julson, T.H. van Andel (Eds.), Proc. ODP Sci. Results 138 (1995) 337–355.
- [3] A.C. Mix, N.G. Pisias, W. Rugh, T. Wilson, A. Morey, T.K. Hagelberg, Benthic foraminifer stable isotope record from site 849 (0–5 Ma): local and global climate changes, in: N.G. Pisias, L.A. Mayer, T.R. Janecek, A. Palmer-Julson, T.H. van Andel (Eds.), Proc. ODP Sci. Results 138 (1995) 371–412.
- [4] R. Tiedemann, M. Sarnthein, N.J. Shackleton, Astronomical timescale for the Pliocene Atlantic $\delta^{18}\text{O}$ and dust flux records from Ocean Drilling Program Site 659, Paleooceanography 9 (1994) 619–638.
- [5] P. Wang, L. Wang, Y. Bian, Z. Jian, Late Quaternary paleoceanography of the South China Sea surface circulation and carbonate cycles, Mar. Geol. 127 (1995) 145–165.
- [6] W.Y. Han, Marine Chemistry of the South China Sea, Science Press, Beijing, 1998, 289 pp. (in Chinese).
- [7] B. Haupt, M. Wiesner, M. Sarnthein, CTD profiles and bottom water temperatures in the South China Sea (SONNE-95 Cruise), in: M. Sarnthein (Ed.), Preliminary Report on SONNE-95 Cruise ‘Monitor Monsoon’ to the South China Sea, Reports, Geol.-Paläontol. Inst. Univ. Kiel, 68 (1994) 181–194.
- [8] P. Wang, Response of Western Pacific marginal seas to glacial cycles paleoceanographic and sedimentological features, Mar. Geol. 156 (1999) 5–39.
- [9] M. Sarnthein, U. Pflaumann, P.X. Wang, H.K. Wong (Eds.), Preliminary Report on SONNE-95 Cruise ‘Monitor Monsoon’ to the South China Sea, in: M. Sarnthein (Ed.), Reports, Geol.-Paläontol. Inst. Univ. Kiel, 1994, 68 pp.
- [10] W. Huang, P. Wang, A quantitative approach to deep-water sedimentation in the South China Sea, Sci. China (Ser. D) 41 (1998) 195–201.
- [11] P. Wang, W.L. Prell, P. Blum et al., Proceedings of the Ocean Drilling Program, Initial Reports 184, Ocean Drilling Program College Station, TX, 2000.
- [12] N.J. Shackleton, M.A. Hall, Stable isotope record of the hole 504 sediments: High resolution record of the Pleistocene, in: J.R. Can, M.G. Langseth et al. (Eds.), DSDP Init. Reports 69 (1983) 431–441.
- [13] W.H. Berger, T. Bickert, H. Schmidt et al., Quaternary oxygen isotope records of pelagic foraminifers: Site 806, Ontong Java Plateau, in: W.H. Berger, L.W. Mayer et al. (Eds.), Proc. ODP Sci. Results 130 (1993) 381–395.
- [14] C.M. Hall, J.W. Farrell, Laser $^{40}\text{Ar}/^{39}\text{Ar}$ age from ash D of ODP Site 758: Dating the Brunhes-Matuyama reversal and oxygen isotope stage 19.1, EOS Trans. AGU 74 (1993) 110.
- [15] W.A. Berggren, D.V. Kent, C.C. Swisher III, M.-P. Aubry, A revised Cenozoic geochronology and chronostratigraphy, in: W.A. Berggren, D.V. Kent, M.-P. Aubry, J. Hardenbol (Eds.), Geochronology, Time Scales and Global Stratigraphic Correlation, SEPM Spec. Publ. 54 (1995) 129–212.
- [16] N.J. Shackleton, J. Imbrie, M.A. Hall, Oxygen and carbon isotope record of East Pacific core V19-30: implications for the formation of deep water in the late Pleistocene North Atlantic, Earth Planet. Sci. Lett. 65 (1983) 233–244.
- [17] N.J. Shackleton, A. Berger, W.R. Peltier, An alternative astronomical calibration of the lower Pleistocene time-scale based on ODP Site 677, Trans. R. Soc. Edinburgh Earth Sci. 81 (1990) 251–261.
- [18] M. Milankovitch, Mathematische Klimalehre und astronomische Theorie der Klimaschwankungen, in: W. Köppen, R. Geiger (Eds.), Handbuch der Klimatologie, Gebrüder Borntraeger, Berlin, I(A), 1930, pp. 1–76.
- [19] J.D. Hays, J. Imbrie, N.J. Shackleton, Variations in the earth’s orbit: pacemaker of the ice ages, Science 194 (1976) 1121–1132.
- [20] W.F. Ruddiman, M.E. Raymo, D.G. Martinson, B.M. Clement, J. Backman, Pleistocene evolution: Northern hemisphere ice sheets and North Atlantic Ocean, Paleooceanography 4 (1989) 353–412.
- [21] Z.L. Ding, Z.W. Yu, N.W. Rutter, T.S. Liu, Towards an orbital time scale for Chinese loess deposits, Quat. Sci. Rev. 13 (1994) 39–70.
- [22] N.J. Shackleton, S. Crowhurst, T. Hagelberg, N. Pisias, D. Schneider, A new late Neogene time scale: Application to Leg 138 sites, in: N.G. Pisias, L.A. Mayer, T.R. Janecek, A. Palmer-Julson, T.H. van Andel (Eds.), Proc. ODP Sci. Results 138 (1995) 73–101.
- [23] A. Berger, M.F. Loutre, Insolation values for the climate

- of the last 10 million years, *Quat. Sci. Rev.* 10 (1991) 297–317.
- [24] J. Laskar, The chaotic motion of the solar system: A numerical estimate of the size of the chaotic zones, *Icarus* 88 (1990) 266–291.
- [25] J. Imbrie, J.D. Hays, D.G. Martinson, A. McIntyre, A.C. Mix, J.J. Morley, N.G. Pisias, W.L. Prell, N.J. Shackleton, The orbital theory of Pleistocene climate: Support from a revised chronology of the marine $\delta^{18}\text{O}$ record, in: A. Berger (Ed.), *Milankovitch and Climate*, D. Reidel, Norwell, MA, 1984, pp. 269–305.
- [26] S.C. Clemens, D.W. Murray, W.L. Prell, Nonstationary phase of the Plio-Pleistocene Asian monsoon, *Science* 274 (1996) 943–948.
- [27] J. Chen, J.W. Farrel, D.W. Murray, W.L. Prell, Timescale and paleoceanographic implications of a 3.6 m.y. oxygen isotope record from the northeast Indian Ocean (Ocean Drilling Program Site 758), *Paleoceanography* 10 (1995) 21–47.
- [28] S.C. Clemens, An astronomical tuning strategy for Pliocene sections: implications for global-scale correlation and phase relationships, *Phil. Trans. R. Soc. London* 357 (1999) 1949–1973.
- [29] Z. Yu, Z. Ding, An automatic orbital tuning method for paleoclimate records, *Geophys. Res. Lett.* 25 (1998) 4525–4528.
- [30] M.E. Raymo, D.W. Oppo, W. Curry, The mid-Pleistocene climate transition: A deep sea carbon isotopic perspective, *Paleoceanography* 12 (1997) 546–559.
- [31] P. Wang, J. Tian, X. Cheng, Transition of Quaternary glacial cyclicity in deep-sea records at Nansha, South China Sea, *Sci. China (Ser. D)* 44 (2001) 926–933.
- [32] S.C. Clemens, W. Prell, D. Murray, G. Shimmield, G. Weedon, Forcing mechanisms of the Indian Ocean monsoon, *Nature* 353 (1991) 720–725.
- [33] P.R. Thompson, A. Bé, J.C. Duplessy, N.J. Shackleton, Disappearance of pink-pigmented *Globigerinoides ruber* at 120,000 yr BP in the Indian and Pacific oceans, *Nature* 280 (1979) 554–558.
- [34] W.A. Berggren, F.J. Hilgen, C.G. Langereis, D.V. Kent, J.D. Obradovich, I. Raffi, M.E. Raymo, N.J. Shackleton, Late Neogene chronology: new perspectives in high-resolution stratigraphy, *Geol. Soc. Am. Bull.* 107 (1995) 1272–1287.
- [35] R.M. Carter, I.N. McCave, C. Richter, L. Carter et al., Proceedings of the Ocean Drilling Program, Initial Reports 181, Ocean Drilling Program, College Station, TX, 1999.
- [36] G.E. Birthfield, Changes in deep-ocean water $\delta^{18}\text{O}$ and temperature from the last glacial maximum to the present, *Paleoceanography* 2 (1987) 431–442.
- [37] R. Zahn, A.C. Mix, Benthic foraminiferal $\delta^{18}\text{O}$ in the oceans temperature-salinity-density field: Constraints on ice age thermohaline circulation, *Paleoceanography* 6 (1991) 1–20.
- [38] T.S. Liu, *loess and the Environment*, China Ocean Press, Beijing, 1985, 215 pp.
- [39] S. Rutherford, S. D’Hondt, Early onset and tropical forcing of 100,000-year Pleistocene glacial cycles, *Nature* 408 (2000) 72–75.
- [40] J.C. Herguera, L.D. Stott, W.H. Berger, Glacial deep-water properties in the west-equatorial Pacific bathyal thermocline near a depth of 2000 m, *Mar. Geol.* 100 (1991) 201–206.